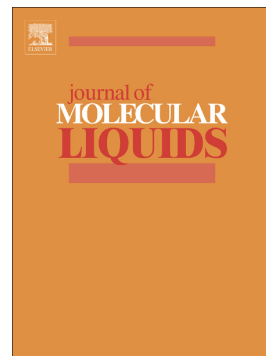


## Accepted Manuscript

Iodine sequestration using cyclophosphazene based inorganic-organic hybrid nanoporous materials: Role of surface functionality and pore size distribution

Raees Muhammad, Paritosh Mohanty



PII: S0167-7322(19)30477-5

DOI: <https://doi.org/10.1016/j.molliq.2019.03.053>

Reference: MOLLIQ 10594

To appear in: *Journal of Molecular Liquids*

Received date: 25 January 2019

Revised date: 7 March 2019

Accepted date: 9 March 2019

Please cite this article as: R. Muhammad and P. Mohanty, Iodine sequestration using cyclophosphazene based inorganic-organic hybrid nanoporous materials: Role of surface functionality and pore size distribution, *Journal of Molecular Liquids*, <https://doi.org/10.1016/j.molliq.2019.03.053>

This is a PDF file of an unedited manuscript that has been accepted for publication. As a service to our customers we are providing this early version of the manuscript. The manuscript will undergo copyediting, typesetting, and review of the resulting proof before it is published in its final form. Please note that during the production process errors may be discovered which could affect the content, and all legal disclaimers that apply to the journal pertain.

# Iodine Sequestration Using Cyclophosphazene Based Inorganic-Organic Hybrid Nanoporous Materials: Role of Surface Functionality and Pore Size Distribution

Raees Muhammad and Paritosh Mohanty\*

Functional Materials Laboratory, Department of Chemistry, Indian Institute of Technology Roorkee, Roorkee, Uttarakhand-247667, India

\*E-mail: pmfcy@iitr.ac.in, paritosh75@gmail.com

**Abstract:** Cyclophosphazene based inorganic-organic hybrid nanoporous materials having triazine and pyrrolic functionality named as HNM-1 and CHNM-1, respectively, with varying nitrogen content, hierarchical pore size and high specific surface area have been explored for iodine sequestration application. The presence of electron rich functionality in the HNM-1 and CHNM-1 provides a large number of active sites for the adsorption of iodine. Maximum gravimetric iodine capture capacity of 223 and 120 wt.% were estimated in HNM-1 and CHNM-1 specimens, respectively, under fuel processing condition i.e. 75 °C and ambient pressure. Moreover, both the specimens have shown very good iodine release behavior in organic solvents. The recyclability of HNM-1 and CHNM-1 for iodine sorption has shown the retention of adsorption capacity by 80 and 86%, respectively, even after five cycles. The iodine sorption both in vapor as well as solution phases is greatly influenced by the nitrogen content and pore size distribution of the framework materials.

**Keywords:** Cyclophosphazene based hybrid materials; iodine sequestration; nanoporous materials; physicochemical properties

## 1. Introduction

Climate crisis owing to uncontrolled anthropogenic release of CO<sub>2</sub> in atmosphere has emerged as one of the greatest threats for society [1],[2],[3],[4]. Hence, the quest for reliable alternate energy source having minimum impact on the environment is very high [5],[6],[7],[8]. Towards this, nuclear energy has been envisioned as the clean and carbon free energy source but the large-scale energy production concerns the release of huge amount of harmful nuclear waste [6],[7],[8],[9]. <sup>129</sup>I is one of the radioactive components of nuclear waste which emerges during the fission of nuclear fuel in nuclear power plant [10],[11]. <sup>129</sup>I has long half-life (1.57 x 10<sup>7</sup> years) and easily incorporate itself into human metabolism and creates health issues [11],[12],[13],[14]. Thus, to develop the nuclear energy at mass scale, there is an urgent need to find the cost-effective materials for efficient capture and storage of iodine which has been a challenging task [11].

Adsorptive removal of iodine has emerged as a more effective solution as compared to caustic and acidic scrubbing methods, as these suffers from recyclability problem [6],[11],[15]. Recently, natural and synthetic silver-exchanged zeolite have been used for the remediation of radioactive iodine in nuclear plant [11],[12]. Although, these materials are hydrothermally stable but their limited iodine uptake has been the major bottleneck towards their utilization under mass scale condition [13]. In addition to above, many more adsorbents like carbonaceous materials [16], porous graphene [17], composites materials [18], metal organic frameworks (MOFs) [6], covalent organic frameworks (COFs) [19],[20], and porous organic polymers [8],[9],[21] have been studied towards adsorptive removal of iodine. The recent studies on iodine capture shed some light on the facts that, the iodine removal capacity is not greatly influenced by only specific surface area, and in fact, the pore surface functionality, pore volume and pore size distribution do

play pivotal role [22],[23],[24]. The enrichment of the frameworks by the heteroatoms have been found to improve the interaction with the iodine and ultimately improvement in the iodine uptake capacity. Liao *et al.* reported that the amine functionalized conjugated microporous polymers demonstrated high iodine uptake (336 wt.%) owing to improved affinity of framework with iodine [13]. Han and coworkers, reported azo bridged porphyrins and phthalocyanine bridged framework having iodine uptake capacity of 220 wt.% [25]. Similarly, Juneta *et al.* have found that presence of imine functionality in the silsesquioxane cores resulted in high iodine uptake capacity (485 wt.%) [26].

As discussed above, the framework enrichment by heteroatoms facilitate iodine uptake owing to better interaction between host and guest, and towards this, use of cyclophosphazene moiety as a source of heteroatoms has been exclusively explored by Mohanty and co-workers [27], [28],[29],[30],[31],[32],[33]. Here cyclophosphazene moiety not only helps in introduction of heteroatoms but also serve as a three-dimensional building block and with its paddle-wheel structure, which creates the void naturally in the framework [27],[28],[29],[30],[31],[32],[33]. Herein, we report the iodine sequestration application of cyclophosphazene based inorganic-organic hybrid nanoporous materials having pyrrolic and triazines moieties with varying nitrogen content and controlled textural properties.

## 2. Materials and Method

### 2.1. Synthesis of compound-I

A common precursor ‘compound-I’ was used for the synthesis of both HNM-1 and CHNM-1 following previous reports [29],[30]. In a typical synthesis, 10 mmol of phosphonitrilic chloride trimer (PNC, 99%, Sigma Aldrich India) dissolved in 50 ml of THF (AR, SRL India) was

condensed with 61 mmol of 4-hydroxybenzaldehyde (99%, Sigma Aldrich India) dissolved in 100 ml THF in presence of 121 mmol of  $K_2CO_3$  (AR, Fisher Scientific India) under argon atmosphere. The reaction was found to be completed after stirring of reaction mixture for 48 h at RT. The detailed synthesis condition and processing/purification of compound-I has been reported elsewhere [29]. The formation of compound-I was confirmed by  $^1H$ ,  $^{13}C$  and  $^{31}P$  NMR spectra [29].  $^1H$  NMR ( $CDCl_3$ ):  $\delta$  9.95 (s), 7.75 (d), 7.17 (d).  $^{13}C$  NMR ( $CDCl_3$ ):  $\delta$  190, 155, 134, 132, 122 and  $^{31}P$  NMR ( $CDCl_3$ ):  $\delta$  7.04.

**2.2. Synthesis of HNM-1:** In a typical synthesis of HNM-1, condensation of 1 mmol of compound-I with 3 mmol of melamine (99%, Sigma Aldrich India) in 30 ml DMSO (AR, Fisher Scientific India) under reflux condition in presence of  $N_2$  atmosphere after 48 h resulted in an off-white powder [29]. The product was washed with methanol, tetrahydrofuran followed by soxhlet extraction with diethyl ether, and dried at 100 °C in hot air oven.

**2.3. Synthesis of CHNM-1:** In a typical synthesis of CHNM-1, 1 mmol of compound-I was condensed with 6 mmol of freshly distilled pyrrole (AR, SRL India) in 5 ml 1,4-Dioxane (AR Fisher Scientific, India) at 70 °C for 1 hour under  $N_2$  atmosphere followed by solvothermal treatment at 180 °C for 48 h, which resulted in a brown monolith [30]. The obtained monolith was washed with methanol and tetrahydrofuran several times followed by drying at 80 °C in vacuum oven.

**2.4. Characterization:** The chemical environment and structural elucidation of the framework materials were carried out using FT-IR (Spectrum Two, PerkinElmer), powder X-ray diffraction (XRD; Ultima IV, Rigaku), elemental analysis (varioMICRO) and XPS (HI-5000 VersaProbe III ULVAC-PHI Inc) analysis. The microstructural characterizations were conducted using field emission scanning electron microscopy (FESEM; MIRA3, TESCAN), and transmission electron

microscopy (TEM; TECNAIG2S-TWIN) instruments. The thermal stability of these framework materials was analyzed using EXSTAR TG/DTA6300 TGA analyzer under argon atmosphere. The textural parameters were estimated by N<sub>2</sub> sorption analysis using Autosorb iQ2 (Quantachrome Instruments, USA) at -196 °C and 1 bar after degassing of the samples at 120 °C for 12 h. The specific surface area (S<sub>A,BET</sub>) was estimated using BET model and the pore size distribution (PSD) was estimated using density functional theory (DFT) model.

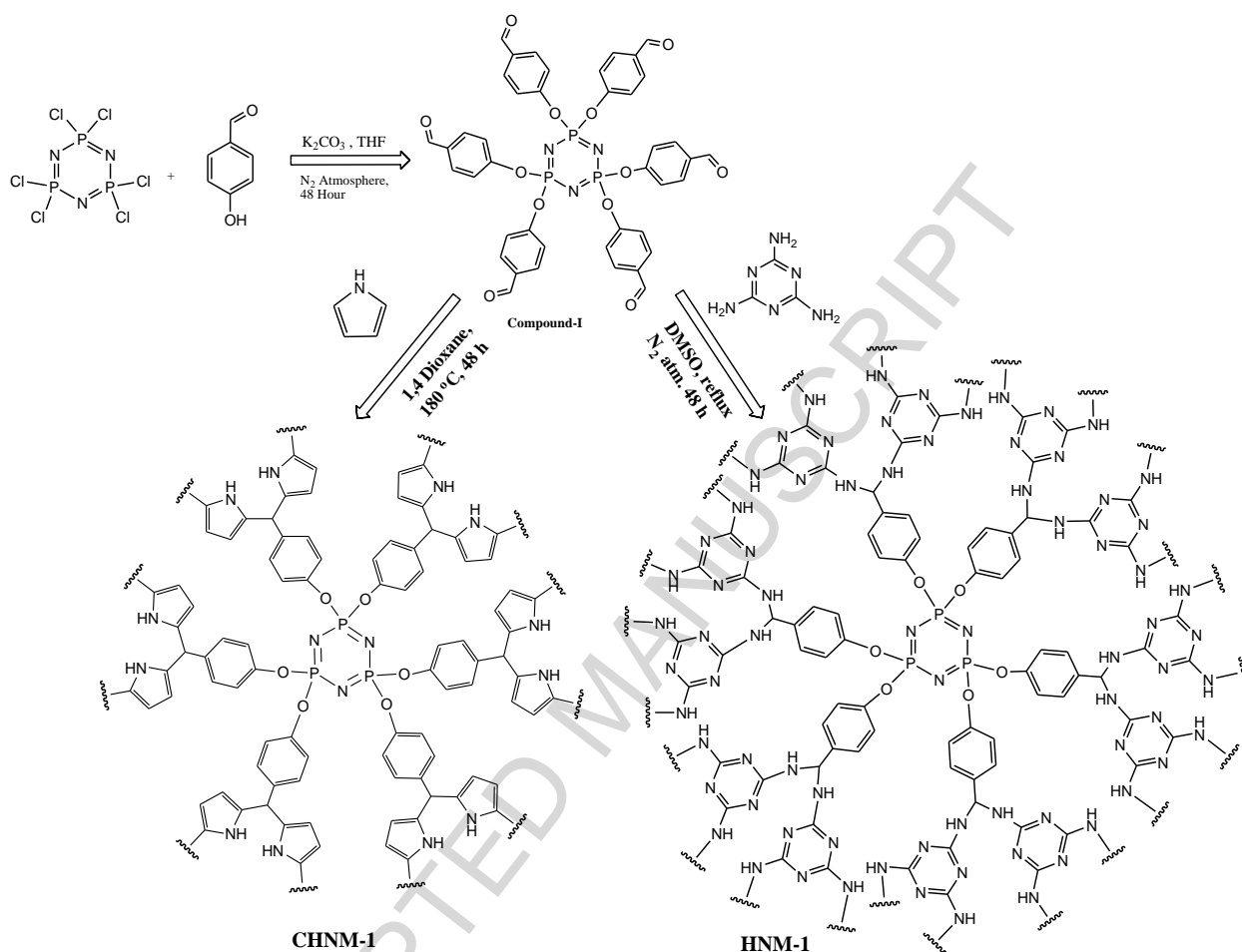
**2.5. Iodine sorption:** The iodine vapor adsorption experiment was conducted using gravimetric analysis under the reaction condition similar to nuclear fuel reprocessing. Before the experiments, both the specimens were activated at 100 °C for 12 h under vacuum. For every experiment, 20 mg of the sample was placed in an open mouth glass vessel which was placed inside the tightly capped glass vessel containing excess of solid Iodine at 75 °C under ambient pressure. The iodine uptake capacity was estimated by the equation (1):

$$\text{Iodine uptake capacity} = \frac{m_t - m_i}{m_i} \times 100 \text{ wt\%} \quad (1)$$

where, m<sub>i</sub> and m<sub>t</sub> are initial mass of the sample and sample mass after time t of the iodine adsorption experiment, respectively.

The iodine adsorption experiment in solution phase was investigated using hexane as a liquid media. In general, 300 ppm iodine solution in hexane was used for all the investigations. About 10 mg of the adsorbents were soaked in the solution for various time intervals at 25 °C. The extent of iodine adsorption from the hexane solution was evaluated by standard UV-visible spectroscopic method using Shimadzu UV-1800 UV-visible spectrophotometer. Irrespective of the adsorption media, the release experiments were carried out in organic media using absolute ethanol as solvent at 25 °C. The recyclability test was carried out by soaking the iodine loaded

specimens in absolute ethanol for 12 h and separated the solid adsorbents using filtration followed by activating the specimens at 100 °C overnight in vacuum.



**Scheme-1.** Reaction scheme for the synthesis of CHNM-1 and HNM-1.

### 3. Results and Discussion

The successful condensation of the compound-I with melamine and pyrrole to form HNM-1 and CHNM-1, respectively, (Scheme-1) was confirmed from the FT-IR and XPS investigations. The observation of bands at  $3440\text{ cm}^{-1}$  due to -N-H stretching (for secondary amine instead of multiplet for primary amine) and  $2925\text{ cm}^{-1}$  due to -C-H stretching of methine linkage, and the absence of aldehyde band at  $\sim 1700\text{ cm}^{-1}$  confirm the condensation in both the cases as shown in

Figure S1 [29],[30],[34]. The multiplet of bands in the region of 1220 to 1130  $\text{cm}^{-1}$  confirms the incorporation of cyclophosphazene ring in the specimens [27],[28],[29],[30]. It is important to note that the band at 1695  $\text{cm}^{-1}$  in CHNM-1 is observed due to  $-\text{C}=\text{N}$  stretching of the pyrrole ring and should not be confused with the aldehyde band [30]. Further, the XPS investigation supports the formation of HNM-1 and CHNM-1 as per the Scheme-1. The XPS survey scans shown in the Figure S2, confirm the presence of P, C, N, and O in framework materials. The in-depth study on the chemical environment of the individual elements i.e. P, C, N and O, was gained by their high-resolution (P 2p, C 1s, O 1s and N 1s) XPS spectra as shown in Figure 1. The C 1s high resolution XPS spectrum for HNM-1 shown in Figure 1(a), has three peaks at 284.8, 285.3 and 288.2 eV owing to the presence of methine, aromatic and triazine carbons, respectively [35],[36],[37],[38]. Similarly, the C 1s XPS spectrum for CHNM-1 also have shown three peaks at 284.8, 285.2 and 286.3 eV, and these could be associated to methine, aromatic and pyrrolic carbons, respectively [37],[39]. The N 1s high resolution XPS spectrum for HNM-1 shown in Figure 1(b) has two peaks at 399.8 and 398.6 eV for the 'N' of the cyclophosphazene ring and triazine ring, respectively, while the N 1s spectrum of CHNM-1 has shown the peaks for the 'N' of cyclophosphazene and pyrrolic ring at 399.0 and 396.7 eV, respectively [36],[37],[38],[39].

The O 1s high resolution XPS spectrum of CHNM-1 has two peaks associated with the 'O' of framework (Scheme-1) and 'O' from the tape used for the sample mounting in XPS analysis (can be seen in the XPS survey scan of silicon tape, Figure S2) at 533.4 and 531.4 eV, respectively [36], but the O 1s high resolution XPS spectrum of HNM-1 in addition to the peaks for 'O' of the framework at 532.9 eV and 'O' of the tape at 531.6 eV, have an extra peak at 530.0 eV originated from the 'O' of DMSO trapped in the pores of the HNM-1, Figure 1(c). The

P 2p high resolution XPS spectra shown in Figure 1(d), have shown a single peak for both HNM-1 and CHNM-1 at 133.4 and 133.1 eV, respectively, indicating the only one type of phosphorous present in the frameworks and incorporation of the cyclophosphazene ring in the framework materials [36].

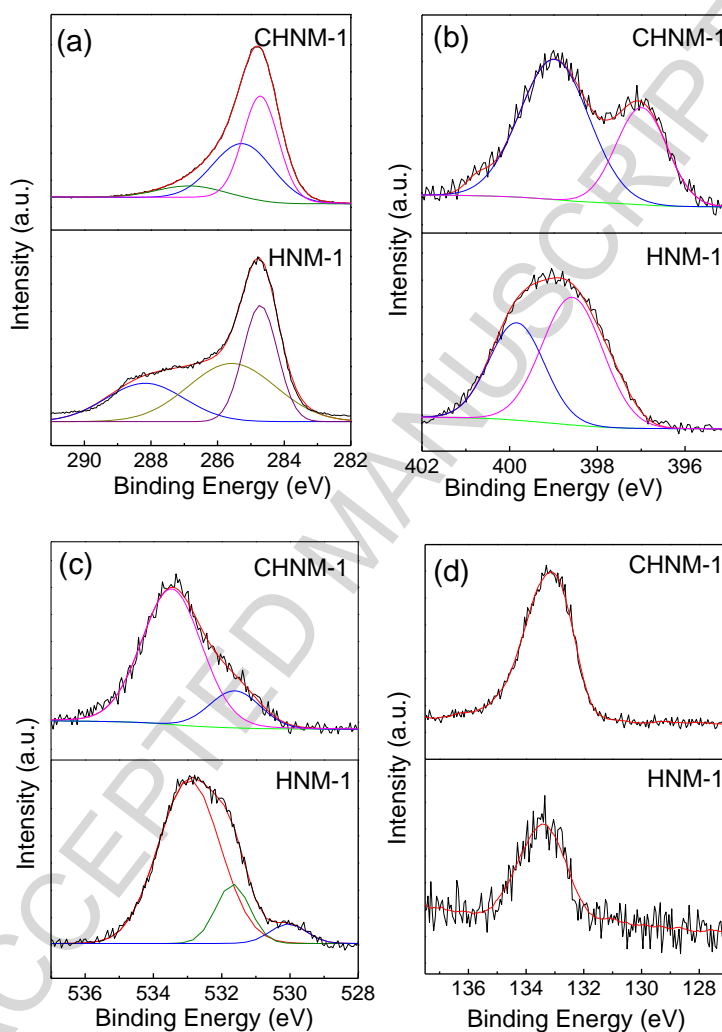


**Figure 1.** XPS high resolution scans; (a) C 1s, (b) N 1s, (c) O 1s and (d) P 2p for HNM-1 and CHNM-1.

The HNM-1 and CHNM-1 were further subjected to elemental analysis. As per the proposed structures in Scheme-1, theoretically, HNM-1 would consist of 41.8 % C, 46.8 % N and 2.9 % H, while CHNM-1 with 70.4 % C, 10.3 % N and 3.9 % H. The experimental

elemental composition was found to be 40.2 % C, 42.2 % N and 4.5 % H for HNM-1, and 62.8 % C, 8.4 % N and 3.5 % H for CHNM-1. The experimentally estimated elemental composition is matching well with the theoretically calculated elemental composition. The thermal gravimetric analysis performed under argon atmosphere indicates that HNM-1 and CHNM-1 are stable up to a temperature of 370 °C, Figure S3. Both of these materials are amorphous in nature as no sharp crystalline peak was observed in the XRD patterns (Figure S4). The microstructural analysis of HNM-1 and CHNM-1 were carried out using FESEM and TEM instruments. Both the samples consist of agglomerated small particles of irregular shapes in the size range of 50 to 200 nm. The TEM images of HNM-1 and CHNM-1 shown in Figure 2(c and d), respectively show the presence of small pores in the nanopore regime. The SAED patterns shown in the inset of figure 2(c & d) indicate that both the materials are amorphous and further corroborate the observation of XRD.

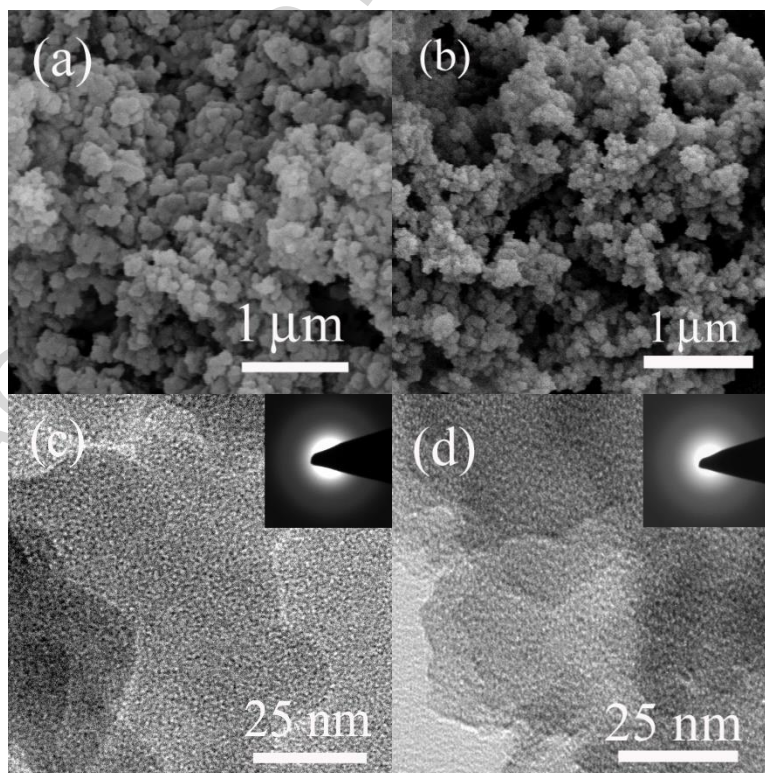


**Figure 2.** FESEM images of (a) HNM-1 and (b) CHNM-1, and TEM images of (c) HNM-1 and (d) CHNM-1. The SAED pattern of samples has been shown in the inset of their respective TEM images.

The textural properties of the HNM-1 and CHNM-1 has been analyzed by  $N_2$  sorption analysis. In Figure 3, a type-I isotherm is observed for HNM-1 while a combination of type-I and type-IV isotherm can be seen for CHNM-1. Both the samples show the remarkable  $N_2$  uptake at low pressure region ( $P/P_0 > 0.1$ ) indicating the presence of micropores. This was further supported by the pore size distribution analysis carried out using DFT method. The majority of pores in HNM-1 are centered at 1.2 nm with significant proportion in ultra-micropore region at 0.65 nm and a very small proportion in mesopore region also [inset of Figure of 3(a)]. The CHNM-1 has two types of pores and these were found to be centered at 1.65 and 3.46 nm [inset of Figure of 3(b)]. The specific surface area estimated by the BET method was found to be 934 and 1283  $m^2 g^{-1}$  for HNM-1 and CHNM-1, respectively (Figure S5). The total pore volume estimated at  $P/P_0$  of 0.90 was calculated to be 0.87 and 1.09  $cm^3 g^{-1}$  for HNM-1 and CHNM-1, respectively.

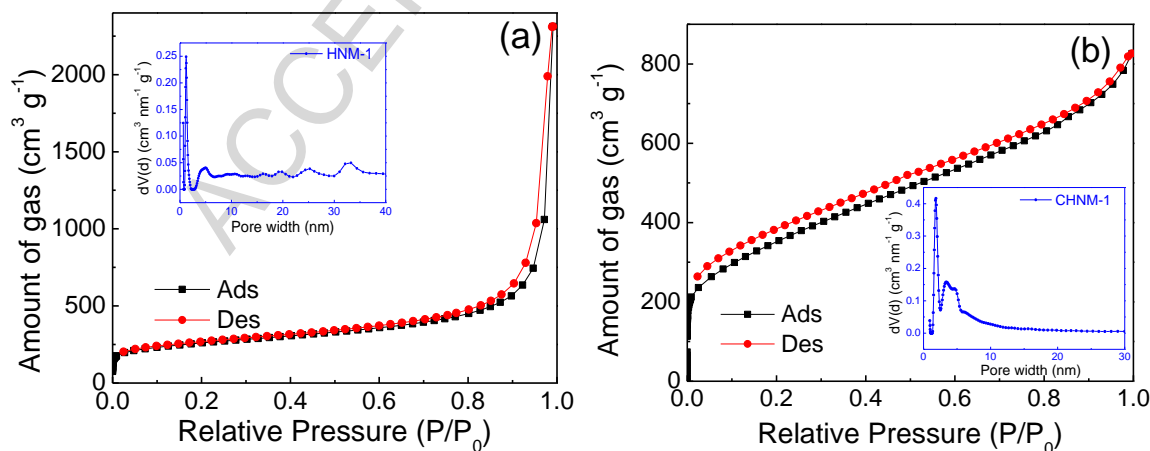


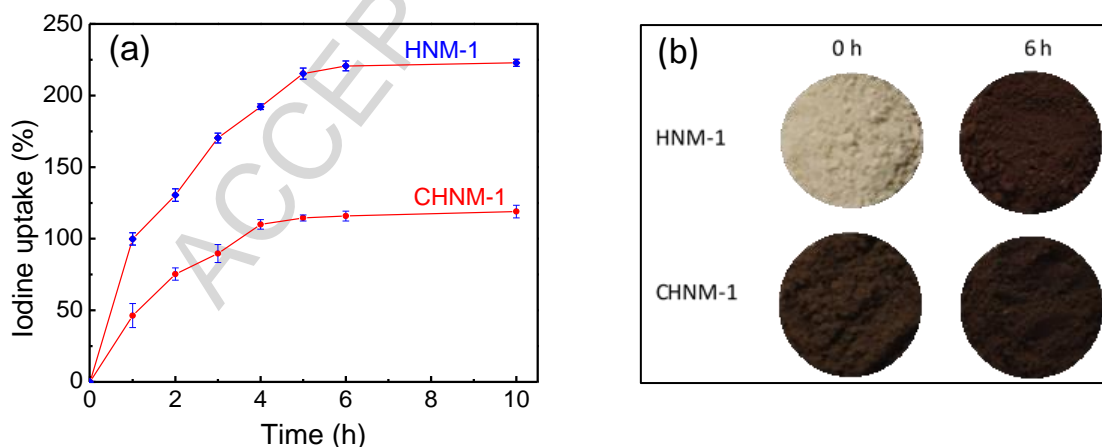
**Figure 3.** Nitrogen sorption isotherms of (a) HNM-1 and (b) CHNM-1. The pore size distribution of HNM-1 and CHNM-1 has been shown in the inset of figure 2(a) and 2(b), respectively.

The presence of heteroatoms such as N, O and P in the framework along with hierarchical pore geometry and controlled textural properties has encouraged us to investigate the iodine adsorption behavior. As discussed above, both HNM-1 and CHNM-1 were employed for the iodine sequestration, both in vapor and in liquid phase. In the vapor phase adsorption, where gravimetric method was used for the estimation of the extent of the iodine adsorption, it has been observed that there is a continuous increase in the mass of the sample over a period of time up to 5 h and 6 h for CHNM-1 and HNM-1, respectively. Beyond this time, there is almost no increase in the mass observed and hence, considered as the saturation is achieved as shown in Figure 4(a). The quicker saturation in case of CHNM-1(5 h) as compared to HNM-1 (6 h) can be attributed to larger pore size which in turn facilitates a better mass transfer. However, it is interesting to see a higher iodine uptake in the HNM-1 (223 wt.%) as compared CHNM-1 (120 wt.%), although, the CHNM-1 has higher  $S_{\text{A}_{\text{BET}}}$  as well as pore volume. This unusual iodine adsorption behavior could be attributed to the significantly larger nitrogen content in HNM-1 (42.2 wt.%) as compared to CHNM-1 (8.4 wt.%), which makes it more electron rich for facilitating the adsorbate-adsorbent interaction. Thus, it could be concluded that the primary factors affecting the iodine adsorption in the present case are the electron rich heteroatom enrichment in the framework as well as the pore size. The iodine capture capacity of HNM-1 is better than many reported adsorbents like SCMP-1 (222 wt.%) [23], NTP (180 wt.%) [21], NIP-CMP (202 wt.%) [9], NBDP-CPP (150 wt.%) [40], S4-LDH (155 wt.%) [41],  $\text{NH}_2$ -HMNOS (202 wt.%) [42], and

comparable to BDP-CPP-2 (223 wt.%) [40], HCMP-3 (336 wt.%) [13], PG-700 (346 wt.%) [17] and AzoPPN (290 wt.%) [25].

The change in color of the samples after iodine adsorption from off white to brown in HNM-1 and brown to dark brown in CHNM-1, as shown in the Figure 4(b), provide compelling evidence of iodine adsorption. It was further confirmed by the comparison of the TGA data of iodine loaded HNM-1 and CHNM-1 named as  $I_2@HNM-1$  and  $I_2@CHNM-1$ , respectively, with the pristine specimens. A significantly higher mass loss was observed for  $I_2@HNM-1$  and  $I_2@CHNM-1$  in the temperature range of 80 to 300 °C as compared to the HNM-1 and CHNM-1, owing to the release of iodine upon heating [Figure 4(c & d)].

The energy dispersive X-ray (EDX) spectroscopy and elemental mapping were used to confirm the presence of iodine in  $I_2@HNM-1$  and  $I_2@CHNM-1$  (Figure S6 and S7). The EDX spectra of  $I_2@HNM-1$  and  $I_2@CHNM-1$  show the peaks for C, N, P, O and I. The peaks of P, C, N and O originated from the framework materials while the peak for I is appeared from the iodine adsorbed on  $I_2@HNM-1$  and  $I_2@CHNM-1$ .



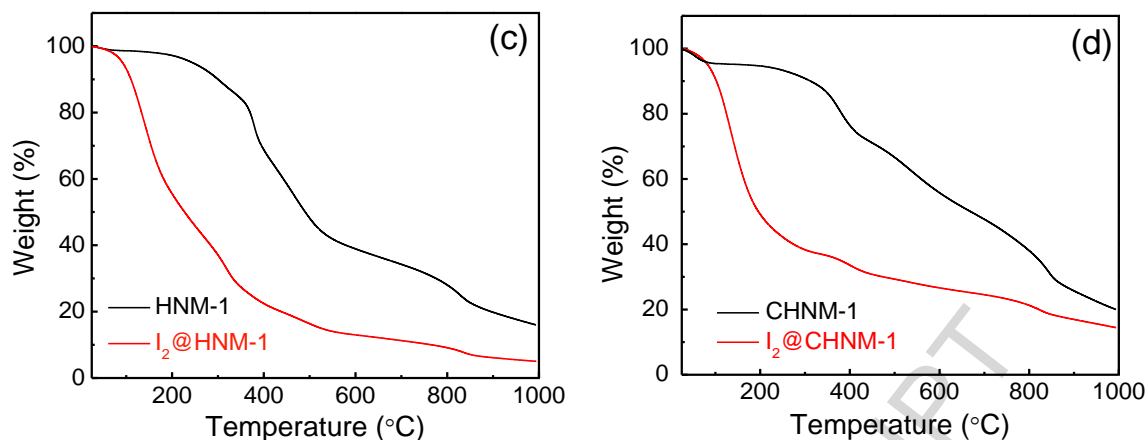


**Figure 4.** (a) Gravimetric iodine uptake of HNM-1 and CHNM-1 estimated at 75 °C. (b) Change in the color of HNM-1 and CHNM-1 after iodine adsorption. TGA of (c) HNM-1 and I<sub>2</sub>@HNM-1, (d) CHNM-1 and I<sub>2</sub>@CHNM-1 under argon atmosphere.

The mechanism of iodine adsorption and its interaction with framework materials, HNM-1 and CHNM-1, were investigated by XPS and Raman spectroscopy. The XPS survey scan of I<sub>2</sub>@HNM-1 and I<sub>2</sub>@CHNM-1 shown in Figure S8, show the peaks for P, C, N & O present in the framework materials in addition to peaks for iodine (I 3d and I 4d). These peaks could be ascribed to the iodine adsorbed on the materials. Further, the high resolution XPS spectra of I 3d<sub>5/2</sub> show the peaks at 618.3 and 620.0 eV for I<sub>2</sub>@HNM-1, and 619.4 and 621.4 eV for I<sub>2</sub>@CHNM-1. These peaks could be ascribed to polyiodide ion I<sub>3</sub><sup>-</sup> and I<sub>5</sub><sup>-</sup>, Figure 5(a & b) [11]. Further, Raman spectra measured by a Renishaw inVia Raman spectrometer at λ<sub>ext</sub> of 514 nm show the bands at 106 and 168 cm<sup>-1</sup> for I<sub>2</sub>@HNM-1 and I<sub>2</sub>@CHNM-1. These peaks further confirm the presence of polyiodide ions [Figure 4 (c & d)] [11],[16],[43],[44].

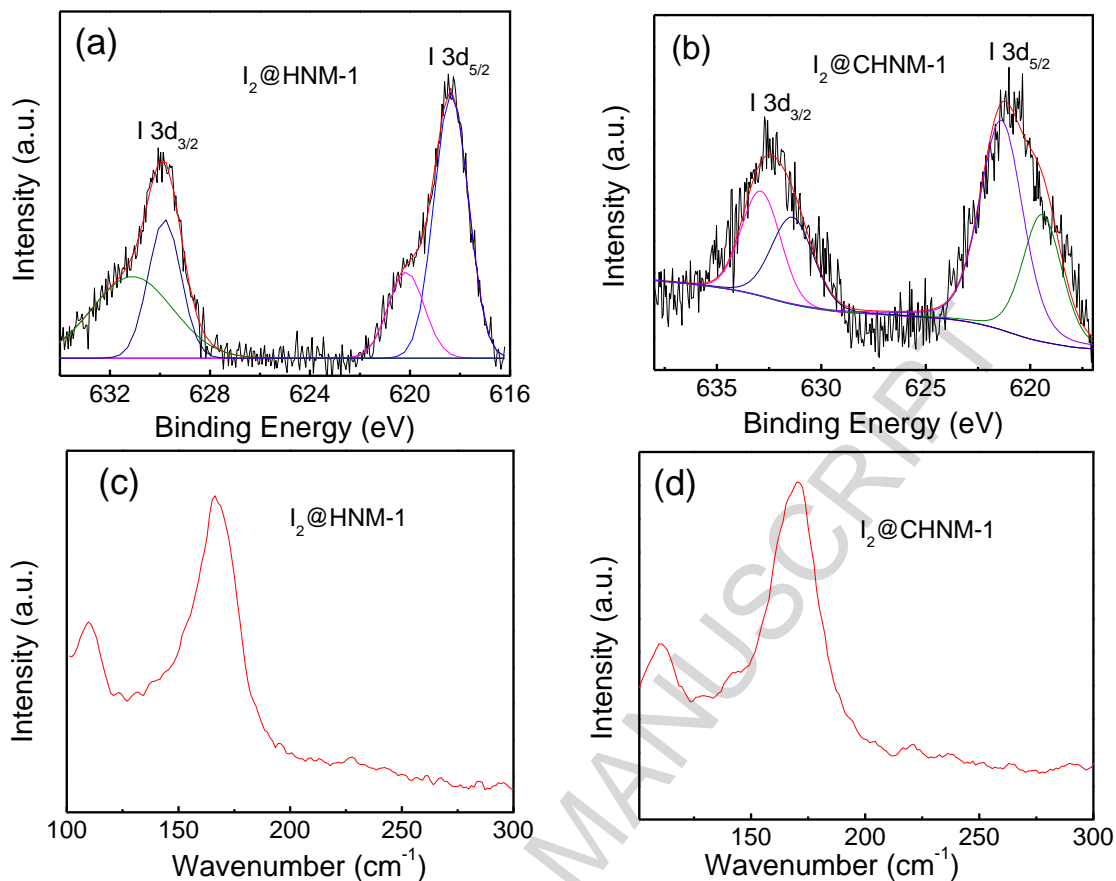


**Figure 5.** I 3d high resolution XPS spectra of (a)  $I_2@HNM-1$  and (b)  $I_2@CHNM-1$ . Raman spectra of (c)  $I_2@HNM-1$ , and (d)  $I_2@CHNM-1$ .

The HNM-1 and CHNM-1 have also been investigated for the iodine adsorption from organic solvents. 10 mg of the adsorbent was soaked in the 300 ppm iodine solution in hexane. The iodine uptake in HNM-1 and CHNM-1 was rapid during the first 30 min of the adsorption experiment and later on the increase in iodine uptake was gradual [Figure 6(a)]. A complete saturation was observed after 720 min. The higher adsorption capacity of HNM-1 as compared to the CHNM-1 led to the complete removal of iodine from the solution leaving behind a completely colorless solution after 12 h, whereas, in CHNM-1, a faint iodine color still exists even after 18 h of the adsorption experiment which is also visible in Figure 6(b & c). The

adsorptive removal efficiency of 98.5 and 87.8 % were estimated for HNM-1 and CHNM-1, respectively.

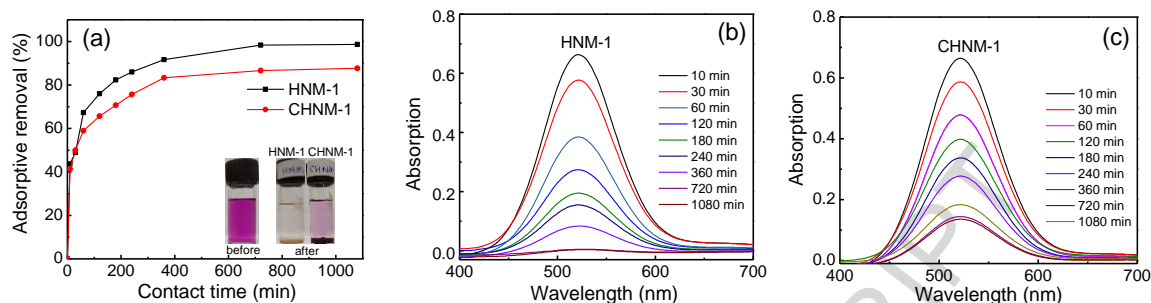


**Figure 6.** (a) Iodine adsorption by HNM-1 and CHNM-1 in hexane solution. (b and c) the absorption of iodine with time. The change in the color of the solution before and after the adsorption is shown in the inset of figure 6(a).

The time dependent release of iodine in ethanol from  $I_2@HNM-1$  and  $I_2@CHNM-1$  is linear with respect to time. The rate of iodine release in CHNM-1 was faster than HNM-1 which further confirms the strong host guest interaction in HNM-1 owing to presence of triazine unit than CHNM-1, Figure S11. The UV-vis spectra shown in Figure S12(a & b) have two maxima at 291 and 360 nm ascribed to polyiodide ion [13],[41]. Further, the recyclability of the HNM-1 and CHNM-1 was carried out. The iodine loaded samples were soaked in absolute ethanol overnight and then dried. After five cycles, the HNM-1 and CHNM-1 have shown the iodine removal efficiency of 80 % and 86%, respectively as shown in Figure S13. The significant loss in iodine capture for HNM-1 after first cycle could be ascribed to stronger affinity of triazine moiety in HNM-1 towards the iodine.

#### 4. Conclusion

In summary, two types of cyclophosphazene based inorganic-organic hybrid nanoporous materials i.e. HNM-1 and CHNM-1 have been explored for iodine adsorption both in vapor and

liquid phase. Both the specimens, due to presence of electron-rich heteroatoms, have shown good affinity towards the iodine which resulted in maximum iodine capture capacity of 223 and 120 wt.% for HNM-1 and CHNM-1, respectively, in vapor phase. The specimens have also shown excellent release of iodine in organic media owing to the hierarchical pore structure of the framework. These specimens have shown the very good adsorption retention capacity (80% for HNM-1, 86% for CHNM-1) even after five cycle. These results demonstrate that the tuning of physicochemical properties such as heteroatom enrichment, pore size and pore volume could pave the way for improved iodine uptake capacity.

#### AUTHOR INFORMATION

##### **Corresponding Author**

\*Email: pmfcy@iitr.ac.in, paritosh75@gmail.com

##### ORCID ID

Raees Muhammad: 0000-0003-3448-5846

Paritosh Mohanty: 0000-0003-2765-0129

##### **Notes**

The authors declare no competing financial interest.

##### **Acknowledgements**

This research was funded by Department of Science and Technology, Govt. of India [Grant No. DST/TDT/TDP-03/2017(G)]

##### **References**

1. S. Solomona, G.-K. Plattnerb, R. Knutti and P. Friedlingstein, Irreversible Climate Change Due to Carbon Dioxide Emissions, *PNAS* 160 (2009) 1704-1709.
2. M. Eddaoudi, L. J. Barbour, CO<sub>2</sub> Separation, Capture and Reuse: A Web Themed Issue, *Chem. Commun.* 51 (2015) 5554-5555.
3. B. Ashourirad, P. Arab, T. Islamoglu, K. A. Cychosz, M. Thommes, H. M. El-Kaderi, A Cost-Effective Synthesis of Heteroatom-doped Porous Carbons as Efficient CO<sub>2</sub> Sorbents, *J. Mater. Chem. A* 4 (2016) 14693-14702.
4. S. R. Venna, M. A. Carreon, Amino-Functionalized SAPO-34 Membranes for CO<sub>2</sub>/CH<sub>4</sub> and CO<sub>2</sub>/N<sub>2</sub> Separation, *Langmuir* 27 (2011) 2888–2894.
5. S. B. Alahakoon, C. M. Thompson, G. Occhialini, R. A. Smaldone, Design Principles for Covalent Organic Frameworks in Energy Storage Applications, *ChemSusChem* 10 (2017) 2116 – 2129.
6. D. Banerjee, X. Chen, S. S. Lobanov, A. M. Plonka, X. Chan, J. A. Daly, T. Kim, P. K. Thallapally, J. B. Parise, Iodine Adsorption in Metal Organic Frameworks in the Presence of Humidity, *ACS Appl. Mater. Interfaces* 10 (2018) 10622–10626.
7. P. R. Deshmukh, Y. Sohn, W. G. Shin, Electrochemical Performance of Facile Developed Aqueous Asymmetric (Fe, Cr)<sub>2</sub>O<sub>3</sub>//MnO<sub>2</sub> Supercapacitor, *Electrochim. Acta* 285 (2018) 381-392.
8. M. Janeta, W. Bury, S. Szafert, Porous Silsesquioxane–Imine Frameworks as Highly Efficient Adsorbents for Cooperative Iodine Capture, *ACS Appl. Mater. Interfaces* 10 (2018) 19964–19973.

9. A. Sigen, Y. Zhang, Z. Li, H. Xia, M. Xue, X. Liu, Y. Mu, Highly Efficient and Reversible Iodine Capture Using a Metalloporphyrin-based Conjugated Microporous Polymer, *Chem. Commun.* 50 (2014) 8495-8498.
10. D. Shetty, J. Raya, D. S. Han, Z. Asfari, J.-S. Olsen, A. Trabolsi, Lithiated Polycalix[4]arenes for Efficient Adsorption of Iodine from Solution and Vapor Phases, *Chem. Mater.* 29 (2017) 8968–8972.
11. J. Huve, A. Ryzhikov, H. Nouali, V. Lali, G. Aug, T. J. Daou, Porous Sorbents for the Capture of Radioactive Iodine Compounds: A Review, *RSC Adv.* 8 (2018) 29248–29273.
12. K. W. Chapman, P. J. Chupas, T. M. Nenoff, Radioactive Iodine Capture in Silver-Containing Mordenites through Nanoscale Silver Iodide Formation, *J. Am. Chem. Soc.* 132 (2010) 8897–8899.
13. Y. Liao, J. Weber, B. M. Mills, Z. Ren, C. F. J. Faul, Highly Efficient and Reversible Iodine Capture in Hexaphenylbenzene-Based Conjugated Microporous Polymers, *Macromolecules* 49 (2016) 6322–6333.
14. Z. Guo, P. Sun, X. Zhang, J. Lin, T. Shi, S. Liu, A. Sun, Z. Li, Amorphous Porous Organic Polymers Based on Schiff-Base Chemistry for Highly Efficient Iodine Capture, *Chem. Asian J.* 13 (2018) 2046 – 2053.
15. N. R. Soelberg, T. G. Garn, M. R. Greenhalgh, J. D. Law, R. Jubin, D. M. Strachan, P. K. Thallapally, Radioactive Iodine and Krypton Control for Nuclear Fuel Reprocessing Facilities, *Sci. Technol. Nucl. Install.* 2013 (2013) 1–12.
16. D. Lia, D. I. Kaplan, A. Sams, B. A. Powell, A. S. Knox, Removal Capacity and Chemical Speciation of Groundwater Iodide ( $I^-$ ) and Iodate ( $IO_3^-$ ) Sequestered by Organoclays and Granular Activated Carbon, *J. Environ. Radioact.* 192 (2018) 505–512.

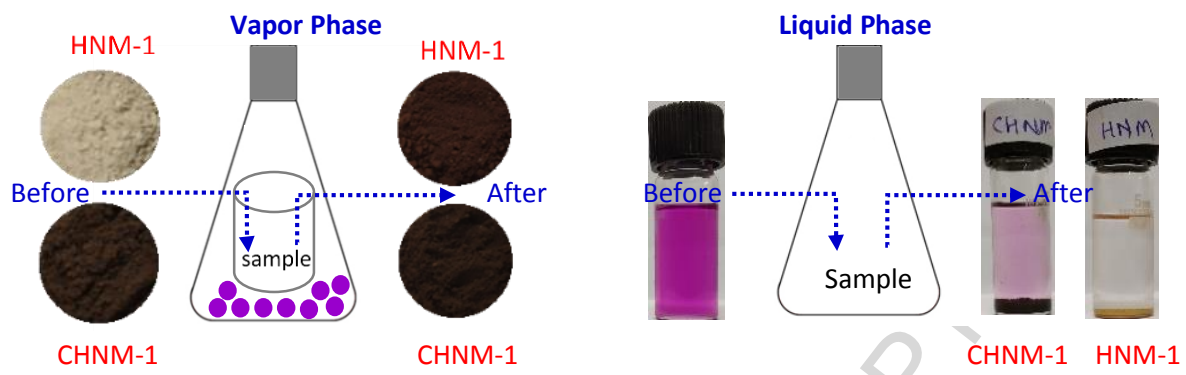
17. H. Sun, P. Mu, H. Xie, Z. Zhu, W. Liang, Z. Zhou, A. Li, Efficient Capture and Reversible Storage of Radioactive Iodine by Porous Graphene with High Uptake, *ChemistrySelect* 3 (2018) 10147–10152.
18. B. Valizadeh, T. N. Nguyen, B. Smit, K. C. Stylianou, Porous Metal–Organic Framework@Polymer Beads for Iodine Capture and Recovery Using a Gas- Sparged Column, *Adv. Funct. Mater.* 28 (2018) 1801596.
19. C. Wang, Y. Wang, R. Ge, X. Song, X. Xing, Q. Jiang, H. Lu, C. Hao, X. Guo, Y. Gao, D. Jiang, A 3D Covalent Organic Framework with Exceptionally High Iodine Capture Capability, *Chem. Eur. J.* 24 (2018) 585 – 589.
20. P. Wang, Q. Xu, Z. Li, W. Jiang, Q. Jiang, D. Jiang, Exceptional Iodine Capture in 2D Covalent Organic Frameworks, *Adv. Mater.* 30 (2018) 1801991.
21. H. Ma, J.-J. Chen, L. Tan, J.-H. Bu, Y. Zhu, B. Tan, C. Zhang, Nitrogen-Rich Triptycene-Based Porous Polymer for Gas Storage and Iodine Enrichment, *ACS Macro Lett.* 5 (2016) 1039–1043.
22. X. Qian, B. Wang, Z.-Q. Zhu, H.-X. Sun, F. Ren, P. Mu, C. Ma, W.-D. Liang, A. Li, Novel N-rich Porous Organic Polymers with Extremely High Uptake for Capture and Reversible Storage of Volatile Iodine, *J. Hazard. Mater.* 338 (2017) 224–232.
23. Q. Xin, Z. Zhu, H. Sun, R. Feng, M. Peng, W. Liang, L. Chen, L. An, Capture and Reversible Storage of Volatile Iodine by Novel Conjugated Microporous Polymers Containing Thiophene Units, *ACS Appl. Mater. Interfaces* 8 (2016) 21063–21069.
24. F. Ren, Z. Zhu, X. Qian, W. Liang, P. Mu, H. Sun, J. Liu, A. Li, Novel Thiophene-bearing Conjugated Microporous Polymer Honeycomb-like Porous Spheres with Ultrahigh Iodine Uptake, *Chem. Commun.* 52 (2016) 9797–9800.

25. H. Li, X. Ding, B.-H. Han, Porous Azo-Bridged Porphyrin–Phthalocyanine Network with High Iodine Capture Capability, *Chem. Eur. J.* 22 (2016) 11863 – 11868.
26. M. Janeta, W. Bury, S. Szafert, Porous Silsesquioxane–Imine Frameworks as Highly Efficient Adsorbents for Cooperative Iodine Capture, *ACS Appl. Mater. Interfaces* 10 (2018) 19964–19973.
27. P. Rekha, R. Muhammad, P. Mohanty, Sonochemical Synthesis of Cyclophosphazene Bridged Mesoporous Organosilicas and Their Application in Methyl Orange, Congo Red and Cr (VI) Removal, *RSC Adv.* 5 (2015) 67690–67699.
28. R. Muhammad, M. Chaudhary, P. Mohanty, Harnessing Electron-Rich Framework in Cyclophosphazene Derived Hybrid Nanoporous Materials for Organocatalytic C–C Bond Formation and Gas Sorption Applications, *J. CO<sub>2</sub> Util.* 25 (2018) 302–309.
29. R. Muhammad, P. Rekha, P. Mohanty, Amino Linked Inorganic–Organic Hybrid Nanoporous Materials (HNMs) for CO<sub>2</sub> Capture and H<sub>2</sub> Storage Applications, *RSC Adv.* 6 (2016) 17100–17105.
30. R. Muhammad, P. Mohanty, Cyclophosphazene-Based Hybrid Nanoporous Materials as Superior Metal-Free Adsorbents for Gas Sorption Applications, *Langmuir* 34 (2018) 2926–2932.
31. P. Mohanty, K. Landskron, Synthesis of Periodic Mesoporous Phosphorus–Nitrogen Frameworks by Nanocasting from Mesoporous Silica Using Melt-Infiltration, *J. Mater. Chem.* 19 (2009) 2400–2406.
32. P. Mohanty, K. Landskron, Simple Systematic Synthesis of Size-Tunable Covalent Organophosphonitridic Framework Nano-and Microspheres, *New J. Chem.* 34 (2010) 215–220.

33. P. Rekha, R. Muhammad, V. Sharma, M. Ramteke, P. Mohanty, Unprecedented Adsorptive Removal of  $\text{Cr}_2\text{O}_7^{2-}$  And Methyl Orange by Using a Low Surface Area Organosilica, *J. Mater. Chem. A* 4 (2016) 17866–17874.
34. R. Muhammad, Jyoti, P. Mohanty, Nitrogen Enriched Triazine Bridged Mesoporous Organosilicas for  $\text{CO}_2$  Capture and Dye Adsorption Applications, *J. Mol. Liq.* 248 (2017) 127–134.
35. J. Zhang, Z. Wang, L. Li, J. Zhao, J. Zheng, H. Cui, Z. Zhu, Self-Assembly of CNH Nanocages with Remarkable Catalytic Performance, *J. Mater. Chem. A* 2 (2014) 8179–8183.
36. Q. Ozay, O. Ozay, Synthesis and Characterization of Drug Microspheres Containing Phosphazene for Biomedical Applications, *Colloid Surf. A-Physicochem. Eng. Asp.* 450 (2014) 99–105.
37. K. Heister, M. Zharnikov, M. Grunze, Characterization of X-ray Induced Damage in Alkanethiolate Monolayers by High-Resolution Photoelectron Spectroscopy, *Langmuir* 17 (2001) 8–11.
38. M. Chaudhary, P. Mohanty, Nitrogen Enriched Polytriazine as a Metal-Free Heterogeneous Catalyst for the Knoevenagel Reaction under Mild Conditions, *New J. Chem.* 42 (2018) 12924–12928.
39. B. C. Patra, S. Khilari, R. N. Manna, S. Mondal, D. Pradhan, A. Pradhan, A. Bhaumik, A Metal-Free Covalent Organic Polymer for Electrocatalytic Hydrogen Evolution, *ACS Catal.* 7 (2017) 6120–6127.
40. Y. Zhu, Y.-J. Ji, D.-G. Wang, Y. Zhang, H. Tang, X.-R. Jia, M. Song, G. Yu, G.-C. Kuang, BODIPY-Based Conjugated Porous Polymers for Highly Efficient Volatile Iodine Capture, *J. Mater. Chem. A* 5 (2017) 6622–6629.

41. S. Ma, S. M. Islam, Y. Shim, Q. Gu, P. Wang, H. Li, G. Sun, X. Yang, M. G. Kanatzidis, Highly Efficient Iodine Capture by Layered Double Hydroxides Intercalated with Polysulfides, *Chem. Mater.* 26 (2014) 7114–7123.
42. Z. He, T. Wang, Y. Xu, M. Zhou, W. Yu, B. Shi, K. Huang, Amino-Functionalized Hollow Microporous Organic Nanospheres for Pd Supported Catalysis and I<sub>2</sub> Uptake, *J. Polym. Sci., Part A: Polym. Chem.* 56 (2018) 2045–2052.
43. T. Geng, S. Ye, Z. Zhu, W. Zhang, Triazine-Based Conjugated Microporous Polymers with N, N, N', N'-Tetraphenyl-1,4-Phenylenediamine, 1,3,5-Tris(diphenylamino)benzene and 1,3,5-Tris[(3-methylphenyl)-phenylamino]benzene as the Core for High Iodine Capture and Fluorescence Sensing of o-Nitrophenol. *J. Mater. Chem. A* 6 (2018) 2808–2816.
44. J. Jeromenok, J. Weber, Restricted Access: On the Nature of Adsorption/Desorption Hysteresis in Amorphous, Microporous Polymeric Materials. *Langmuir* 29 (2013) 12982–12989.

**Graphic Image**



**Highlights**

- Cyclophosphazene based hybrid materials have been explored for iodine sequestration
- Iodine sequestration both in liquid and vapor phase have been studied
- Maximum iodine adsorption capacity of 223 wt.% have been estimated
- The physicochemical properties played the pivotal role in iodine sequestration

ACCEPTED MANUSCRIPT